Nano Research 2018, 11(12): 6190–6196
https://doi.org/10.1007/s12274-018-2136-3
Research Article
ISSN 1998-0124
CN 11-5974/O4

Tuning the morphology of chevron-type graphene nanoribbons by choice of annealing temperature

Yun Cao[1,§], Jing Qi[1,§], Yan-Fang Zhang[1,§], Li Huang[1], Qi Zheng[1], Xiao Lin[1], Zhihai Cheng[2], Yu-Yang Zhang[1,3], Xinliang Feng[4,5] (✉), Shixuan Du[1] (✉), Sokrates T. Pantelides[1,3], and Hong-Jun Gao[1]

[1] *Institute of Physics & University of Chinese Academy of Sciences, Chinese Academy of Sciences, Beijing 100190, China*
[2] *Department of Physics, Renmin University of China, Beijing 100872, China*
[3] *Department of Physics and Astronomy and Department of Electrical Engineering and Computer Science, Vanderbilt University, Nashville, Tennessee 37235, USA*
[4] *Center for Advancing Electronics Dresden (cfaed) & Department of Chemistry and Food Chemistry, Technische Universität Dresden, D-01069 Dresden, Germany*
[5] *School of Chemistry and Chemical Engineering, Shanghai Jiao Tong University, Shanghai 200240, China*
[§] *Yun Cao, Jing Qi, and Yan-Fang Zhang contributed equally to this work.*

Received: 28 April 2018
Revised: 4 June 2018
Accepted: 20 June 2018

KEYWORDS

chevron-type graphene nanoribbon,
C–S bond cleavage,
negative differential resistance,
scanning tunneling microscopy (STM),
noncontact atomic force microscopy (NC-AFM),
first-principles calculations

ABSTRACT

Bottom-up synthesis of graphene nanoribbons (GNRs) by surface-assisted polymerization and cyclodehydrogenation of specifically designed precursor monomers has been shown to yield precise edges and doping. Here we use a precursor monomer containing sulfur atoms to fabricate nanostructures on a Au(111) surface at different annealing temperatures. The nanostructures have distinct configurations, varying from sulfur-doped polymers to sulfur-doped chevron-type GNRs (CGNRs) and, finally, pristine graphene nanoribbons with specific edges of periodic five-member carbon rings. Non-contact atomic force microscopy provides clear evidence for the cleavage of C–S bonds and formation of pristine CGNRs at elevated annealing temperatures. First-principles calculations show that the CGNRs exhibit negative differential resistance.

Address correspondence to Shixuan Du, sxdu@iphy.ac.cn; Xinliang Feng, feng@mpip-mainz.mpg.de

1 Introduction

Existence of Dirac cones at the Fermi energy and the concomitant absence of an energy gap in the band structure of graphene limits its use in semiconductor devices, even though graphene has numerous excellent properties [1–3]. Cutting graphene into graphene nanoribbons (GNRs) resolves this problem because the band gap values of GNRs depend on the GNR width and choice of doping atoms [4–7]. There are two basic experimental methods to fabricate GNRs, top-down and bottom-up.

Using the top-down method, GNRs with desirable lengths can be obtained by etching a graphene layer [8, 9]. However, in such GNRs, the edges and doping sites are difficult to control, which causes variations in their electronic structures and limits their applications [10, 11]. On the contrary, the bottom-up method is used to fabricate GNRs with atomically precise widths [12, 13], edges [14], and dopants [4–7, 15, 16]. This method has led to significant progress in the precise design and synthesis of GNRs, such as 7/13 armchair GNRs (AGNRs, straight AGNRs with seven or thirteen carbon atoms in the width direction) and chevron-type GNRs (CGNRs), both pristine and doped with N or S atoms [5, 7, 15, 16]. For the choice of dopant atom, sulfur is particularly important because it has been shown to have an effect on the band gap. However, sulfur atoms can detach from precursors on metal substrates [17], which impacts the final configuration of GNRs and therefore requires further investigation.

In this letter, we report the bottom-up fabrication of nanostructures using sulfur-substituted precursor molecules and their detailed characterization by low-temperature scanning tunneling microscopy (STM) and noncontact atomic force microscopy (NC-AFM). We also report pertinent density-functional-theory (DFT)-based calculations. After annealing precursor molecules on a Au(111) substrate at 550 K for 5 min, C–Br bonds break and sulfur-doped linear polymers are formed. After further annealing at 680 K for 30 min, sulfur-doped CGNRs are fabricated. With subsequent annealing at an even higher temperature (800 K for 1 h), pristine CGNRs with five-member edge rings are obtained, which result from full desulfurization of edges. The desulfurization process is similar to what has been observed in organic molecules on Pt or Au surfaces [17–19]. Calculations reveal that the CGNRs exhibit negative differential resistance, which has potential applications in amplification [20], digital applications [21], and oscillators [22]. This work reveals the importance of precise control over temperature during the fabrication of sulfur-doped CGNRs using the bottom-up method with sulfur-containing precursors.

2 Results and discussion

The basic steps involved in the experiment are depicted in Fig. 1. The precursor, 6,11-dibromo-1,4-diphenyl-2,3-dithenoyltriphenylene, is thermally deposited from a home-built Knudsen cell evaporator onto a Au(111) substrate kept at room temperature (Fig. 1(a)). Then, the substrate is annealed to 550 K for 5 min, the temperature at which the precursors polymerize to form linear polymer chains through C–Br bond cleavage (Ullmann debromination [12]) and biradical C–C bonding between neighboring precursors (Fig. 1(b)). Further annealing at 680 K for 30 min induces full cyclization through a dehydrogenation process (Fig. 1(c)) along with partial C–S bond cleavage. At this stage, only some of the S atoms are detached, resulting in

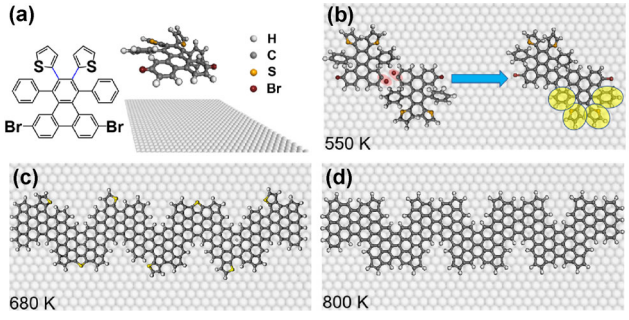

Figure 1 Basic steps of the experiment process. (a) Structure model of the monomer. (b) After the monomers are deposited on Au(111) and annealed at 550 K for 5 min, the monomers undergo the Ullmann debromination and polymerization process. The small red ellipse depicts the C–Br bond cleavage and biradical C–C bonding. The yellow ellipse depicts the out-of-plane thiophene rings and phenyl rings. (c) After further annealing at 680 K for 30 min, the sample undergoes cyclodehydrogenation and partial desulfurization processes, resulting in S-doped CGNRs with nonuniform segments. (d) After further annealing at 800 K for 1 h, the CGNR is fully desulfurized, giving rise to pristine CGNR with periodic five-member carbon rings on the edges.

nonuniform CGNRs with different edge modifications. After the final subsequent annealing at a temperature of 800 K for 1 h, fully desulfurized CGNRs are fabricated (Fig. 1(d)).

Figure 2(a) shows that the precursor monomers adsorb on the elbow sites of the reconstructed Au(111) surface. The monomers polymerize to a long molecular chain by C–Br bond cleavage and neighboring phenyl C–C bonding after annealing at 550 K for 5 min. In the corresponding STM and NC-AFM images (Figs. 2(b) and 2(c)), the outer protrusions at the polymer's edges result from the out-of-plane thiophene rings and phenyl rings (as shown by the yellow eclipses in Fig. 1(b)). Due to the C–C single bonds (in blue in Fig. 1(a)) between the thiophene (phenyl) rings and the backbone of the molecular chain, the thiophene rings and phenyl rings are able to rotate, resulting in out-of-plane configurations. The remaining parts of the molecule compose a big aromatic system lying relatively flat on the substrate.

The molecular chains are fully cyclized to form sulfur-doped CGNRs after further annealing at 680 K for 30 min. The whole ribbon comprises a big aromatic unit that lies flat on the substrate after the dehydrogenation and cyclization process. The flat morphology can be clearly resolved in both the STM image (Fig. 2(d)) and NC-AFM image (Fig. 2(e)). However, the CGNRs contain nonuniform segments at this stage, as clearly seen in the NC-AFM image in Fig. 2(e). This inhomogeneity is mainly caused by two effects. First, the C–C single bonds connecting the two thiophene rings to the backbone may rotate, resulting in different configurations when the precursors land on the substrate. Second, at this annealing temperature (~ 680 K), some of the C–S bonds in the thiophene rings are cleaved by noble-metal catalysis [17–19, 23], which further complicates the configurations. Although noble-metal-catalyzed C–S bond cleavage in thiophene rings is widely accepted, it is the first time that the cleavage is observed in real space using the NC-AFM technique.

Three typical segments in sulfur-doped CGNRs after partial C–S bond cleavage are shown in Fig. 3. In Fig. 3(a), the right thiophene ring remained intact, while the S atom in the left thiophene ring was fully detached. The carbon atoms in the left thiophene

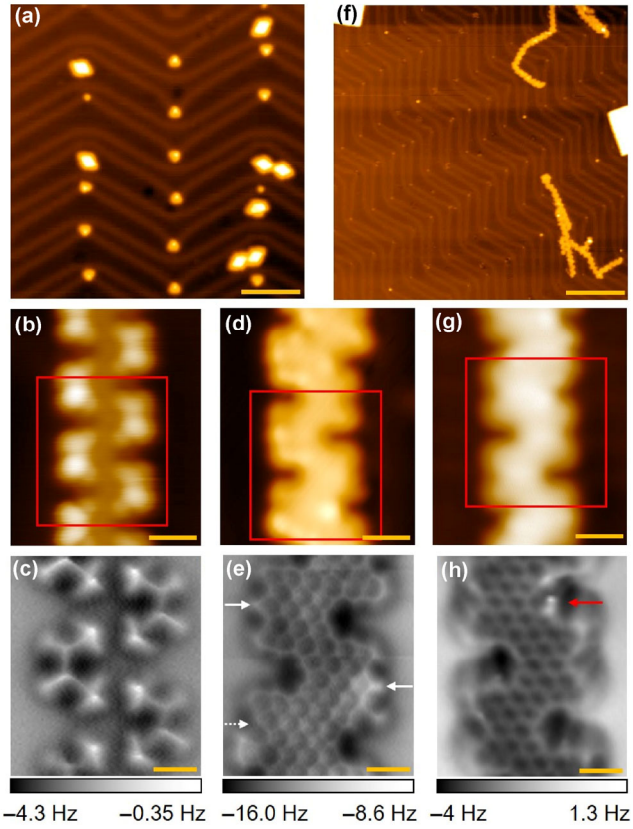

Figure 2 Precursors and ribbons after being annealed at different temperatures. (a) Large-scale STM image shows that molecule monomers preferentially adsorb at elbow positions of Au(111) reconstructed surfaces. (b), (d), and (g) STM images (sample bias = −1 V, tunneling current = 20 pA) at annealing temperatures of 550, 680, and 800 K, respectively. (c), (e), and (h) Corresponding AFM images, which were recorded with a CO-terminated tip and amplitude set point = 100 pm. (b) and (c) Linear polymer that only undergoes the polymerization process after annealing at 550 K for 5 min. (d) and (e) After further annealing the sample at an elevated temperature at 680 K for 30 min, the ribbon is fully cyclized and composed of different segments. (f) Large-scale STM image of CGNRs after further annealing at 800 K for 1 h. (g) and (h) Ribbon segments formed at 800 K. Scale bars: (a) 10 nm, ((b), (d), and (g)) 1 nm, ((c), (e), and (h)) 4 Å, and (f) 20 nm.

rings bonded to adjacent phenyl carbons resulting in a five-membered carbon ring on the shoulder (the red one in the schematic of Fig. 3(a)). Therefore, the segment has one thiophene ring and one five-membered carbon ring on the edge. In Fig. 3(b), the left thiophene ring underwent the same process as in Fig. 3(a), resulting in a five-membered carbon ring on the shoulder (red). While in the right thiophene ring, one C–S bond had been broken and the remainder reformed a new thiophene ring (green) and a five-membered

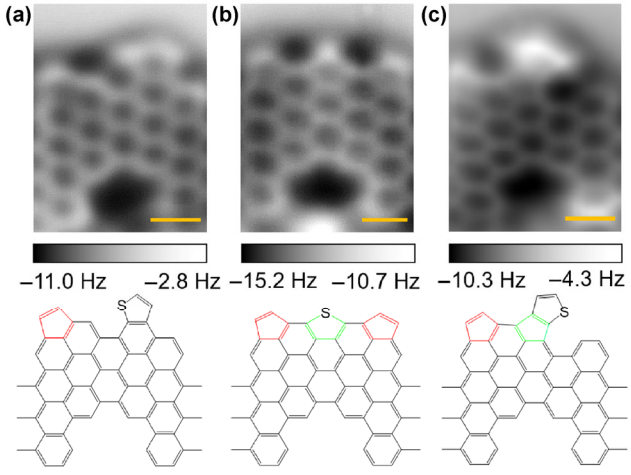

Figure 3 (a)–(c) NC-AFM images and structure models of three typical segments after sample is annealed at 550 K for 5 min and 680 K for 30 min. The segments in (a) and (b) have the same configurations as indicated by the dashed arrow and solid arrows in Fig. 2(e), respectively. Scale bars: 2 Å.

carbon ring (red in Fig. 3(b)). In Fig. 3(c), the left thiophene ring underwent the same process as its counterpart in Fig. 3(a), while the right thiophene ring bonded to the left part of the segment, forming a new five-membered ring (green in Fig. 3(c)), different from the previous two cases. These distinctive segments confirm that at 680 K, C–S bond cleavage has a non-negligible impact on the final configurations of the product structure.

With subsequent annealing at 800 K for 1 h, the sulfur-doped CGNRs undergo full desulfurization, giving rise to undoped, i.e., pristine, CGNRs, as shown in Figs. 2(f)–2(h). Figure 2(f) shows a large-area STM image of CGNRs. Figures 2(g) and 2(h) display enlarged STM and AFM images of a CGNR, respectively, which clearly show fully desulfurized segments in the CGNR. Note that although the segments share the feature of five-membered edge rings, they are not uniform in the bay regions, as indicated by the red arrow in Fig. 2(h). The defective bay regions are probably due to detached S atoms or missing hydrogen atoms during the desulfurization and cyclodehydrogenation processes. As it is very challenging to resolve hydrogen atoms in the plane of the polycyclic aromatic hydrocarbons, even with a CO tip [24, 25], we are still unable to determine the exact configuration of the defects.

To further examine possible applications of the final pristine CGNR, we constructed a CGNR with periodic five-membered carbon rings on the edges and investigated its electronic structure and transport properties by density functional theory (DFT) calculations. The geometric structures are shown in Fig. 4(a). The black rectangle represents the unit cell used in the band-structure calculations. Figure 4(b) presents the band structure of CGNRs, revealing that they are semiconducting with a bandgap of 0.82 eV.

The transport properties of a Au(111)-CGNR-Au(111) device, shown schematically as an inset in Fig. 4(c), are presented in Fig. 4(c). The *I*–*V* curve describes the behavior of the specific GNR length employed. Furthermore, the calculations are performed at 0 K and remain valid as coherent transport at finite but low temperatures, as long as the mean-free path imposed by phonon scattering is much longer than the device length. Figure 4(c) reveals a nonzero current at energies smaller than the bandgap, most likely from tunneling due to the very short device length, imposed by computational limitations.

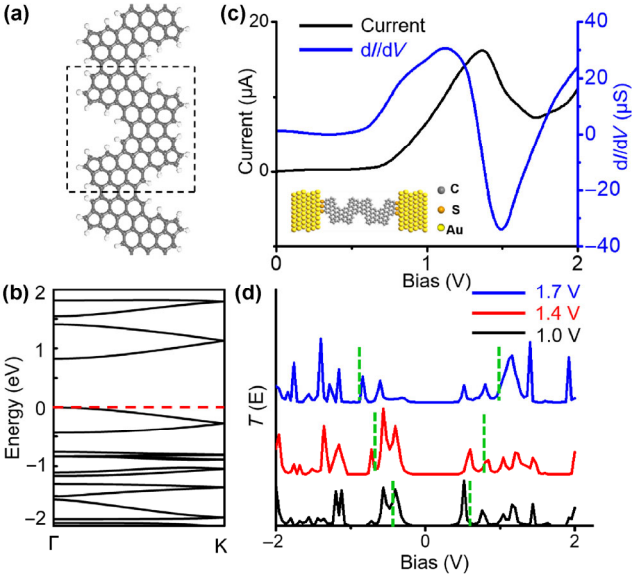

Figure 4 Band structure and transport properties of CGNR by first-principles calculations. (a) Geometric structure of CGNR with a black dashed rectangle showing the unit cell. (b) Band structure of pristine CGNR, with a red dashed line showing the Fermi energy. (c) *I*–*V* (black line) and d*I*/d*V* curve (blue line) of CGNR under bias voltage from 0 to 2.0 V for the device shown in the inset (sulfur atoms are used to connect the CGNR and gold electrodes in the device model, gray: C, orange: S, yellow: Au). (d) Transmission coefficients of the CGNR device under bias voltages of 1.0, 1.4, and 1.7 V, respectively. Dashed green lines show the integration bias window under each bias voltage.

A remarkable property of the CGNR device is the deep valley of a current at 1.7 V (the blue curve in Fig. 4(c)), which indicates that the device has negative differential resistance (NDR). This NDR effect is widely reported in both GNR-based devices [26, 27] and other conventional devices [21, 28, 29]. The dI/dV curve in Fig. 4(c) shows the NDR with a value of around –30 μS. According to the Landauer-Buttiker formula [30] $I = \frac{2e}{h}\int_{\mu_1}^{\mu_2} T(E,V)\mathrm{d}E$, the current is the integral of the transmission coefficient in a bias window (chemical potential difference between the two electrodes under bias voltage equal to $\mu_2 - \mu_1$). The evolution of the transmission coefficient in the bias windows (green dashed lines) for the CGNR is depicted in Fig. 4(d), which shows that the integration in the bias windows increases from 1.0 to 1.4 V and decreases from 1.4 to 1.7 V, resulting in the NDR effect.

3 Conclusions

In conclusion, we have successfully fabricated sulfur-doped CGNRs and pristine CGNRs using a precursor monomer containing S atoms by increasing the annealing temperature stepwise. We present a full characterization of sulfur-doped CGNRs, which consist of nonuniform segments due to C–S bond cleavage. At an elevated annealing temperature, fully desulfurized pristine CGNRs are fabricated, which have the potential to feature negative differential resistance as revealed by transport calculations. This work demonstrates that precise control over temperature is important for the fabrication of CGNRs using S-substituted precursors and that C–S bond cleavage must be considered at elevated temperatures.

4 Methods

4.1 Experimental methods

The experiments were conducted in an ultra-high vacuum low-temperature STM/AFM system with a base pressure higher than 3.0×10^{-10} mbar. All the images (STM and AFM) were acquired with CO-functionalized tips to enhance resolution [31, 32]. The measurements were conducted at 4.5 K. The Au(111) substrate was treated by repeated cycles of standard Ar^+ sputtering and annealing at 750 K to obtain an atomically flat clean surface.

4.2 Theoretical methods

First-principles calculations based on DFT were performed using the local density approximation (LDA) [33]. The structural optimization and the band-structure were carried out using the Vienna Ab initio Simulation Package (VASP) [34, 35]. The energy cutoff was 400 eV. The structures were relaxed until the residual forces were smaller than 0.01 eV/Å. The reciprocal space was sampled by the point during the optimization process. The band structure was calculated along the high-symmetry directions in the Brillouin zone.

The electronic transport properties of the two GNRs were calculated using DFT and the non-equilibrium Green's function (NEGF) method [36] as implemented in the ATK software [37, 38]. The GNRs and Au(111) two-probe systems consisted of three parts: the left and right electrodes and the central scattering region. The left and right electrodes contained two identical 6 × 9 Au(111) surfaces and three layers of Au(111) atoms to accommodate the GNR-electrode coupling interactions, while the center device region contained a CGNR with length of around 4.0 nm. S atoms were used to connect the CGNR and Au electrodes. Double-ζ plus polarization orbitals (DZP) were used for the core GNRs atoms, and single-ζ plus polarization orbitals (SZP) were used for the Au electrode atoms. The Hamiltonian overlaps and electronic densities were evaluated in a real space grid defined with a plane wave cutoff of 150 Ry to achieve a balance between the calculation efficiency and accuracy. Transmission coefficients were calculated using standard Green's function methods. The *I-V* characteristics were calculated using the Landauer-Buttiker formula [30].

Acknowledgements

We acknowledge the financial support from the National Key Research and Development Projects of China (No. 2016YFA0202300), the National Basic Research Program of China (No. 2013CBA01600), the National Natural Science Foundation of China (Nos. 61390501,

51572290, 61306015, 61471337, 51325204, and 11604373), the Chinese Academy of Sciences (Nos. 1731300500015 and XDB07030100), and the CAS Pioneer Hundred Talents Program. A portion of the research was performed in CAS Key Laboratory of Vacuum Physics. Work at Vanderbilt (S. T. P. and Y. Y. Z.) was supported by the US Department of Energy under grant DE-FG02-09ER46554 and by the McMinn Endowment.

References

[1] Castro Neto, A. H.; Guinea, F.; Peres, N. M. R.; Novoselov, K. S.; Geim, A. K. The electronic properties of graphene. *Rev. Mod. Phys.* **2009**, *81*, 109–162.

[2] Geim, A. K.; Novoselov, K. S. The rise of graphene. *Nat. Mater.* **2007**, *6*, 183–191.

[3] Lv, R. T.; Terrones, M. Towards new graphene materials: Doped graphene sheets and nanoribbons. *Mater. Lett.* **2012**, *78*, 209–218.

[4] Bronner, C.; Stremlau, S.; Gille, M.; Brauβe, F.; Haase, A.; Hecht, S.; Tegeder, P. Aligning the band gap of graphene nanoribbons by monomer doping. *Angew. Chem., Int. Ed.* **2013**, *52*, 4422–4425.

[5] Cai, J. M.; Pignedoli, C. A.; Talirz, L.; Ruffieux, P.; Söde, H.; Liang, L. B.; Meunier, V.; Berger, R.; Li, R. J.; Feng, X. L. et al. Graphene nanoribbon heterojunctions. *Nat. Nanotechnol.* **2014**, *9*, 896–900.

[6] Kawai, S.; Saito, S.; Osumi, S.; Yamaguchi, S.; Foster, A. S.; Spijker, P.; Meyer, E. Atomically controlled substitutional boron-doping of graphene nanoribbons. *Nat. Commun.* **2015**, *6*, 8098.

[7] Zhang, Y.; Zhang, Y. F.; Li, G.; Lu, J. C.; Lin, X.; Du, S. X.; Berger, R.; Feng, X. L.; Müllen, K.; Gao, H. J. Direct visualization of atomically precise nitrogen-doped gravphene nanoribbons. *Appl. Phys. Lett.* **2014**, *105*, 023101.

[8] Han, M. Y.; Özyilmaz, B.; Zhang, Y. B.; Kim, P. Energy band-gap engineering of graphene nanoribbons. *Phys. Rev. Lett.* **2007**, *98*, 206805.

[9] Wang, X. R.; Dai, H. J. Etching and narrowing of graphene from the edges. *Nat. Chem.* **2010**, *2*, 661–665.

[10] Han, P.; Akagi, K.; Canova, F. F.; Mutoh, H.; Shiraki, S.; Iwaya, K.; Weiss, P. S.; Asao, N.; Hitosugi, T. Bottom-up graphene-nanoribbon fabrication reveals chiral edges and enantioselectivity. *ACS Nano* **2014**, *8*, 9181–9187.

[11] Yang, W. L.; Lucotti, A.; Tommasini, M.; Chalifoux, W. A. Bottom-up synthesis of soluble and narrow graphene nanoribbons using alkyne benzannulations. *J. Am. Chem. Soc.* **2016**, *138*, 9137–9144.

[12] Cai, J. M.; Ruffieux, P.; Jaafar, R.; Bieri, M.; Braun, T.; Blankenburg, S.; Muoth, M.; Seitsonen, A. P.; Saleh, M.; Feng, X. L. et al. Atomically precise bottom-up fabrication of graphene nanoribbons. *Nature* **2010**, *466*, 470–473.

[13] Chen, Y. C.; de Oteyza, D. G.; Pedramrazi, Z.; Chen, C.; Fischer, F. R.; Crommie, M. F. Tuning the band gap of graphene nanoribbons synthesized from molecular precursors. *ACS Nano* **2013**, *7*, 6123–6128.

[14] Ruffieux, P.; Wang, S. Y.; Yang, B.; Sánchez-Sánchez, C.; Liu, J.; Dienel, T.; Talirz, L.; Shinde, P.; Pignedoli, C. A.; Passerone, D. et al. On-surface synthesis of graphene nanoribbons with zigzag edge topology. *Nature* **2016**, *531*, 489–492.

[15] Nguyen, G. D.; Tom, F. M.; Cao, T.; Pedramrazi, Z.; Chen, C.; Rizzo, D. J.; Joshi, T.; Bronner, C.; Chen, Y. C.; Favaro, M. et al. Bottom-up synthesis of $N = 13$ sulfur-doped graphene nanoribbons. *J. Phys. Chem. C* **2016**, *120*, 2684–2687.

[16] Zhang, Y. F.; Zhang, Y.; Li, G.; Lu, J. C.; Que, Y. D.; Chen, H.; Berger, R.; Feng, X. L.; Müllen, K.; Lin, X. et al. Sulfur-doped graphene nanoribbons with a sequence of distinct band gaps. *Nano Res.* **2017**, *10*, 3377–3384.

[17] Wang, L. D.; He, W.; Yu, Z. K. Transition-metal mediated carbon-sulfur bond activation and transformations. *Chem. Soc. Rev.* **2013**, *42*, 599–621.

[18] Zhong, C. J.; Porter, M. D. Evidence for carbon-sulfur bond cleavage in spontaneously adsorbed organosulfide-based monolayers at gold. *J. Am. Chem. Soc.* **1994**, *116*, 11616–11617.

[19] Kundu, S.; Brennessel, W. W.; Jones, W. D. C–S bond activation of thioesters using platinum(0). *Organometallics* **2011**, *30*, 5147–5154.

[20] McWhorter, A. L.; Foyt, A. G. Bulk gaas negative conductance amplifiers. *Appl. Phys. Lett.* **1966**, *9*, 300–302.

[21] Broekaert, T. P. E.; Brar, B.; van der Wagt, J. P. A.; Seabaugh, A. C.; Morris, F. J.; Moise, T. S.; Beam, E. A.; Frazier, G. A. A monolithic 4-bit 2-Gsps resonant tunneling analog-to-digital converter. *IEEE J. Solid-St. Circ.* **1998**, *33*, 1342–1349.

[22] Brown, E. R.; Söderstrom, J. R.; Parker, C. D.; Mahoney, L. J.; Molvar, K. M.; McGill, T. C. Oscillations up to 712 GHz in InAs/AlSb resonant-tunneling diodes. *Appl. Phys. Lett.* **1991**, *58*, 2291–2293.

[23] Hua, R. M.; Takeda, H.; Onozawa, S. Y.; Abe, Y.; Tanaka, M. Palladium-catalyzed thioesterification of alkynes with O-methyl S-phenyl thiocarbonate. *J. Am. Chem. Soc.* **2001**, *123*, 2899–2900.

[24] Pavliček, N.; Majzik, Z.; Collazos, S.; Meyer, G.; Pérez, D.; Guitián, E.; Peña, D.; Gross, L. Generation and characterization of a meta-aryne on Cu and NaCl surfaces. *ACS Nano* **2017**,

11, 10768–10773.

[25] Schuler, B.; Fatayer, S.; Mohn, F.; Moll, N.; Pavliček, N.; Meyer, G.; Peña, D.; Gross, L. Reversible bergman cyclization by atomic manipulation. *Nat. Chem.* **2016**, *8*, 220–224.

[26] Ren, H.; Li, Q. X.; Luo, Y.; Yang, J. L. Graphene nanoribbon as a negative differential resistance device. *Appl. Phys. Lett.* **2009**, *94*, 173110.

[27] Nguyen, V. H.; Bournel, A.; Dollfus, P. Large peak-to-valley ratio of negative-differential-conductance in graphene p-n junctions. *J. Appl. Phys.* **2011**, *109*, 093706.

[28] Galperin, M.; Nitzan, A.; Ratner, M. A. The non-linear response of molecular junctions: The polaron model revisited. *J. Phys.: Condens. Matter* **2008**, *20*, 374107.

[29] Migliore, A.; Nitzan, A. Irreversibility and hysteresis in redox molecular conduction junctions. *J. Am. Chem. Soc.* **2013**, *135*, 9420–9432.

[30] Datta, S. *Quantum Transport: Atom to Transistor;* Cambridge University Press: Cambridge, UK, 2005.

[31] Bartels, L.; Meyer, G.; Rieder, K. H. Controlled vertical manipulation of single CO molecules with the scanning tunneling microscope: A route to chemical contrast. *Appl. Phys. Lett.* **1997**, *71*, 213–215.

[32] Gross, L.; Mohn, F.; Moll, N.; Liljeroth, P.; Meyer, G. The chemical structure of a molecule resolved by atomic force microscopy. *Science* **2009**, *325*, 1110–1114.

[33] Perdew, J. P.; Zunger, A. Self-interaction correction to density-functional approximations for many-electron systems. *Phys. Rev. B* **1981**, *23*, 5048–5079.

[34] Kresse, G.; Furthmuller, J. Efficiency of *ab-initio* total energy calculations for metals and semiconductors using a plane-wave basis set. *Comp. Mater. Sci.* **1996**, *6*, 15–50.

[35] Kresse, G.; Furthmüller, J. Efficient iterative schemes for *ab initio* total-energy calculations using a plane-wave basis set. *Phys. Rev. B* **1996**, *54*, 11169–11186.

[36] Taylor, J.; Guo, H.; Wang, J. *Ab initio* modeling of quantum transport properties of molecular electronic devices. *Phys. Rev. B* **2001**, *63*, 245407.

[37] Brandbyge, M.; Mozos, J. L.; Ordejón, P.; Taylor, J.; Stokbro, K. Density-functional method for nonequilibrium electron transport. *Phys. Rev. B* **2002**, *65*, 165401.

[38] Soler, J. M.; Artacho, E.; Gale, J. D.; García, A.; Junquera, J.; Ordejón, P.; Sánchez-Portal, D. The SIESTA method for *ab initio* order-*N* materials simulation. *J. Phys.: Condens. Matter* **2002**, *14*, 2745–2779.